applied sciences

MDPI

Article

A Comparative Numerical Analysis on the Effect of Welding Consumables on the Ballistic Resistance of SMAW Joints of Armor Steel

Ambuj Saxena [1], Shashi Prakash Dwivedi [1], Shubham Sharma [2,*], Vishal Shankar Srivastava [1], Gursharan Singh [2], Jujhar Singh [2], Somnath Chattopadhyaya [3] and Catalin I. Pruncu [4,5,*]

1 Department of Mechanical Engineering, G.L. Bajaj Institute of Technology and Management, Greater Noida 201306, India; ambuj.saxena1@gmail.com (A.S.); spdglb@gmail.com (S.P.D.); vishalcool4186@gmail.com (V.S.S.)
2 Department of Mechanical Engineering, IK Gujral Punjab Technical University, Main Campus-Kapurthala Road, Jalandhar 144603, India; gursharan635@gmail.com (G.S.); jujharsingh2085.2085@gmail.com (J.S.)
3 Department of Mechanical Engineering, Indian Institute of Technology (ISM), Dhanbad 826004, India; somnathchattopadhyaya@iitism.ac.in
4 Department of Mechanical Engineering, Imperial College London, Exhibition Road, London SW7 2AZ, UK
5 Design, Manufacturing & Engineering Management, University of Strathclyde, Glasgow G1 1XJ, UK
* Correspondence: shubham543sharma@gmail.com or shubhamsharmacsirclri@gmail.com (S.S.); c.pruncu@imperial.ac.uk or catalin.pruncu@strath.ac.uk (C.I.P.)

Citation: Saxena, A.; Dwivedi, S.P.; Sharma, S.; Srivastava, V.S.; Singh, G.; Singh, J.; Chattopadhyaya, S.; I. Pruncu, C. A Comparative Numerical Analysis on the Effect of Welding Consumables on the Ballistic Resistance of SMAW Joints of Armor Steel. *Appl. Sci.* **2021**, *11*, 3629. https://doi.org/10.3390/app11083629

Academic Editor: Filippo Berto

Received: 15 March 2021
Accepted: 13 April 2021
Published: 17 April 2021

Abstract: In the present investigation, a comparative study of ballistic impact behavior of Armox 500T (base metal) and its weldments prepared by low hydrogen ferrite (weldment-1) and austenitic stainless steel (weldment-2) consumables against 7.62 AP bullet has been performed with the help of finite element analysis code Abaqus 2017. Further, the result is validated with the experimental results. The experiment has been performed on the base metal, weldment-1, and weldment-2 against 7.62 AP bullet. Further, a two-dimensional explicit model has been developed for given purpose to simulate the bullet penetration at such high strain rate (10^3 s^{-1}). Both bullet and plate are considered as deformable. Experimental results revealed that the depth of penetration in the base metal, weldment-1, and weldment-2 is 10.93, 13.65, and 15.20 mm respectively. Further computational results revealed that the depth of penetration of base metal, weldment-1, and weldment-2 is 10.11, 12.87, and 14.60 mm, respectively. Furthermore, weldment-1 shows more resistance against 7.62 AP bullet than weldment-2 in experimentation as well as FEA results. The percentage difference between experimental and FEA results are less than 10% which shows the prediction capability of FEA models. A feasibility analysis has been presented for using the welding consumables to weld the Armox 500T plate. Finally, in terms of ballistic resistance, the low hydrogen ferrite consumables are more appropriate than austenitic stainless-steel electrodes.

Keywords: Armox 500T; SMAW welding; ballistic testing; JC model; FEA; high strain rate

1. Introduction

Armor steel is mostly used for the fabrication of armor plates for military structures, main battle tanks (MBT), and armament combat vehicles (ACV) [1,2]. Saxena et al. [3–6] revealed that armor steels possess high density with excellent mechanical properties, i.e., ultra-high strength and high hardness to resist penetration against projectiles and shaped charge threats. Armox 500T steel is one such quenched and tempered steel having a martensitic structure subject to high loading rates in applications such as ballistic impact, collision, detonation etc. The shield metal arc welding (SMAW) process is mostly recommended to fabricate thick armor steel sections like turret and ship hulls, landing gears, earth moving, mining equipment, mortar casings, armored personnel carrier, cash in transit

vehicle, patrol vehicle etc. [1,3]. Further, recent investigations [3–6] revealed that austenitic stainless steel (ASS) and low hydrogen ferrite (LHF) consumables are widely used as electrodes in the SMAW process. The phenomenon of ballistic impact on different metal targets against a projectile is associated with different types of effect, e.g., viscous and thermal. Nowadays, the simulation of ballistic processes like bullet penetration plays a very crucial role in obtaining a detailed understanding of the deformation process at such high strain rates (10^3 s^{-1}). High velocity impact and penetration problems include large deformation, erosion, high strain rate dependent non-linear material behavior, and fragmentation. Therefore, it is important to model the penetration where above effects are considered. Numerical methods and corresponding computing technologies have been evolved to the level where complex deformation and penetration pattern during ballistic impact can be accurately predicted. Further to simulate such a type of impact like bullet penetration requires detailed information of target plate and projectile material in the form of different material models Johnson–Cook (JC) hardening model, JC damage model, ductile damage model, etc. The JC material and damage model are capable to predict deformation behavior in the ballistic impact process, which comes under the category high strain rate and high temperature [7].

Saxena et al. [3–6] revealed in their studies the choice welding consumables affected the mechanical properties of the fusion zone because formation of different type of microstructures.

Reddy et al. [8] investigated the ballistic performance of armor steel and its gas metal arc welding (GMAW) weldments against 7.62 AP bullet. The weldments were prepared with different welding speed and heat inputs. Further the results revealed that the weldments with greater heat input values show poor ballistic performance.

Reddy et al. [9] analyzed the ballistic performance of armor steel weldments prepared with shielded metal arc welding (SMAW), gas tungsten arc welding (GTAW), and flux cored arc welding (FCAW). Further results revealed that SMAW weldments exhibited the highest ballistic limit among other weldments. In addition, the FCAW weldments show the least ballistic limit among other weldments.

Pramanick et al. [10] investigated the ballistic performance of armor grade quenched and tempered AISI 4340 SMAW weldments with different microstructure constituents and concluded that lower bainite along with retained austenite show maximum toughness at −40 °C and room temperature.

Iqbal et al. [11] determine the JC hardening and failure material model constant for armor grade Armox 500T and 7.62 AP bullet material. Further, they developed a FEA model based on the material model constants and validated it with experimental results. The developed FEA model successfully predicted the plastic flow behavior of target plate and 7.62 AP bullet within 10% accuracy.

FEA models of armor grade steel SMAW weldments are rarely available in the literature. Hence, there is a need for a FEA model which can successfully predict the plastic deformation and failure of armor grade steel weldments.

Further, the above investigations are limited to the armor steel weldments of a thickness between 5 and 10 mm only. The thickness of the main battle tanks (MBT) armor plate is lies between 20 and 60 mm. Further, the armor plate has been joined in the tank with the help of SMAW. In the present study, an experimental and computational analysis has been performed to simulate the influence of ASS and LHF welding consumables on the ballistic performance of multi-pass SMAW joints against 7.62 AP. The 7.62 AP bullet is mostly used in different types of mini machine guns and widely used in war zones for attacking.

2. Experimental Details

2.1. Material

Armox 500T was manufactured with the mixing of cast slabs and chemical ores. It was rolled and water quenched at 1523 and 1273 K respectively. Further, it was tempered within the temperature range of 473–773 K [2–6]. The SMAW process has been adopted to weld the single V groove butt joint of two 25 mm thick armor plate with each dimen-

sion of 150 × 200 × 25 mm. The SMAW process has been performed with the help of austenitic stainless steel (ASS) (Weldment-1) and low hydrogen ferrite (LHF) (Weldment-2) consumable electrodes. The chemical composition of weldment-1 and weldment-2 has been mentioned in Table 1, which was also taken from Saxena et al. [3–6].

Table 1. Chemical composition (wt. %) of test samples under investigation [3].

Material	C	Si	Mn	P	S	Cr	Ni	Mo	N	B	Fe
Base metal	0.31	0.265	0.86	0.019	0.007	0.60	0.82	0.24	-	0.005	Balance
Weldment-1	0.06	0.58	0.85	0.017	0.012	0.04	0.03	0.015	0.018	-	Balance
Weldment-2	0.05	0.51	1.18	0.018	0.06	18.03	9.45		0.04	-	Balance

2.2. Penetration Test with 7.62 AP Bullet

The bullet penetration test has been performed in the armament testing center of Defence Metallurgical Research Laboratory, Hyderabad (India). A schematic diagram of the bullet penetration test is shown in Figure 1.

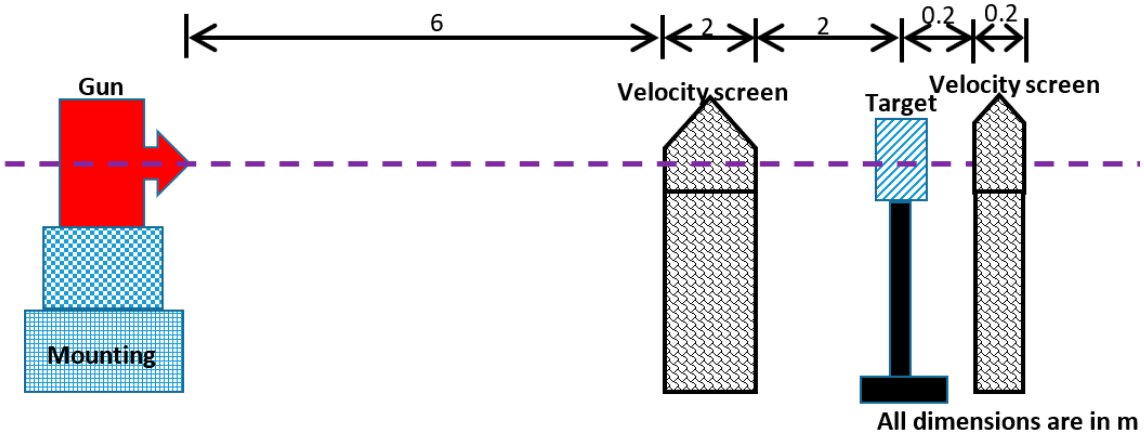

Figure 1. Schematic diagram of bullet penetration test.

The schematic diagram of experimental setup use for bullet penetration is shown in Figure 1. A 7.62 mm armor-piercing hard steel core projectile (7.62 AP) covered with a copper case was used in the ballistic experiments. The projectile core without copper case has dimensions of Φ7.62 × 11.43 mm (Figure 2) and a mass of 5.34 g, while the core with the copper case has a mass of 10.4 g [12]. Bullet shots were fired on the target plates (base metal, weldment-1 and weldment-2) with the recorded impact velocity of 820 m/s.

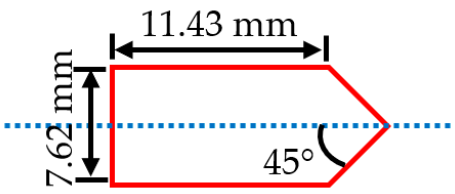

Figure 2. Schematic diagram of 7.62 AP Bullet steel core [13].

The target plate dimensions are 200 × 150 × 25 mm. The distance between the target plate and riffle muzzle is 10 m in the present experiment. At the time of the firing, the gun with accessories like receiver and firing mechanism is fastened on a mounting with holding device and adaptors for providing stability to the 7.62 AP bullets. The gun and target plate planes are leveled with 1.5 m distance above the ground level. The 7.62AP bullet is attached with a cartridge which is put in the firing mechanism for providing the

power for movement of the bullet after triggering the gun. The rifling in the bore section helps to spin the bullet inside the bore and reduce the wobbling.

There are two velocity probes. The first placed before the target for measuring the impact velocity at the distance of 6 m from the gun barrel, and the second is situated behind the target at the distance of 0.2 m for measuring residual velocity. The velocity probes are connected to the multi-channel electronic timer for measuring the time in travel a fixed distance. Aluminum foils are used to fabricate the velocity probes and it is placed in a wooden frame with cardboard. In the present investigation, the target plates thickness is 25 mm, and it cannot be fully penetrated by 7.62 AP bullets. Further, the results come in the form of depth of penetration (D.O.P).

Børvik et al. [13] observed that, when only the steel hard core was used as a projectile, the ballistic limit dropped by 3–5%, which indicates that modeling only the steel hard core in FE simulations of a bullet penetrating armor steel targets is conservative. Hence, in the present numerical simulation's investigations only steel core of 7.62 AP bullet has been used.

2.3. Fractographical Analysis

The fracture surface microstructural analysis of base metal, weldment-1, and weldment-2 plate has been performed with the help of optical microscopy. Optical microstructures were taken from semi-automatic microscope (Make: Leica Microsystems).

3. Finite Element Analysis Simulation

3.1. Input Material Properties

The mechanical properties of investigated material have been taken from the literature directly to perform the numerical simulation. The mechanical properties of Armox 500T and 7.62 AP bullet has been taken from Iqbal et al. [11] and Saxena et al. [12] studies and mentioned in Table 2. The multi-pass SMAW procedure of 25 mm thickness Armox 500T plate with ASS and LHF consumables are explain by Saxena et al. [3–6] in detail. Further, the mechanical properties of SMAW joints prepared with LHF consumables (Weldment-1) and ASS consumables (Weldment-2) are also taken from Saxena's [12] research work and mentioned in Table 2.

Table 2. Material parameters of investigated materials used in Numerical Simulations.

Description	Notation	Base Metal [11]	Weldment-1 [12]	Weldment-2 [12]	7.62 AP Bullet [11]
Modulus of elasticity	E (N/m^2)	201×10^9	201×10^9	200×10^9	200×10^9
Poisson's ratio	ν	0.33	0.3	0.32	0.3
Density	ρ	7850	7850	7850	7850
Yield stress constant	A (N/m^2)	1372.488×10^6	331.47×10^6	345.19×10^6	1657.71×10^6
Strain hardening constant	B (N/m^2)	835.022×10^6	331.47×10^6	523.900×10^6	$20{,}855.6 \times 106$
	n	0.2467	0.4454	0.2819	0.651
Viscous effect	C	0.0617	0.122	0.096	0.0076
Thermal sensitivity	m	0.84	1	1	0.35
Reference strain rate	$\dot{\varepsilon}_0$ (s^{-1})	1	10^{-3}	10^{-3}	1
Melting temperature	T_m (K)	1800	1800	1800	1800
Reference temperature	T_{ref} (K)	293	293	293	293
Fracture strain constant	D_1	0.04289	0.0510	0.0463	0.0301
	D_2	2.1521	2.0426	2.341	0.0142
	D_3	−2.7575	−2.8342	−2.567	−2.192
	D_4	−0.0066	−0.0509	−0.0408	0.0
	D_5	0.86	0	0	0.35

Table 2. *Cont.*

Description	Notation	Base Metal [11]	Weldment-1 [12]	Weldment-2 [12]	7.62 AP Bullet [11]
Inelastic heat fraction	χ	0.9	0.9	0.9	0.9
Specific heat	C_p (J/Kg K)	455	455	455	455
Thermal conductivity	K (W/m k)	47	47	47	47

3.2. JC Hardening Model

In the JC constitutive material model [14], three fundamental material responses, namely strain hardening, strain-rate effects, and thermal softening, are combined in a multiplicative manner as given in Equation (1).

$$\sigma = (A + B\varepsilon^n)\left(1 + C\, ln\dot{\varepsilon}^*\right)\left(1 - (T^*)^m\right) \quad (1)$$

where σ is true stress, A, B, and C are experimentally determined material constants. A is the basic yield stress, B (strength coefficient) and n (strain hardening exponent) are the strain-hardening effects, ε is the accumulated true plastic strain, C is the strain rate constant, $\dot{\varepsilon}^* = \dot{\varepsilon}/\dot{\varepsilon}_0$ is the dimensionless strain rate ($\dot{\varepsilon}$ is the strainrate, while $\dot{\varepsilon}_0$ is the reference strain rate), and T^* is homologous temperature given by:

$$T^* = \frac{T - T_{ref}}{T_m - T_{ref}} \quad (2)$$

where T_m, T, T_{ref} are melting, current, and reference temperatures, respectively. The current temperature values is taken between the range of 293 K to 1173 K [12]. m is the thermal softening fraction. The JC hardening model parameters for base metal, weldment-1, weldment-2 and 7.62 AP steel bullet core has been taken from the Iqbal et al. [11] and Saxena et al. [12] studies as mentioned in Table 2.

3.3. JC Damage Model

Johnson and Cook [15] broadened the fracture criterion suggested by Hancock and Mackenzie [16] to make the failure strain sensitive to stress triaxiality, temperature, and strain rate. The damage parameter D is defined as:

$$D = \sum \frac{\Delta\varepsilon}{\varepsilon_f} \quad (3)$$

where $\Delta\varepsilon$ is an increment of the true plastic strain, ε_f is the equivalent true plastic strain at failure, and the summation is performed over all increments of deformation. The strain at failure (ε_f) depends on stress triaxiality, strain rate, and temperature and can be expressed as

$$\varepsilon_f = [D_1 + D_2 exp(D_3\sigma^*)]\left[1 + D_4 \ln\frac{\dot{\varepsilon}}{\dot{\varepsilon}_0}\right][1 + D_5 T^*] \quad (4)$$

where D_1, D_2, D_3, D_4, and D_5 are material constants, $\sigma^* = \sigma_m/\sigma_{eq}$ is the stress triaxiality ratio and σ_m is the mean stress. JC failure for base metal, weldment-1, weldment-2, and 7.62 AP steel bullet core has been taken from the Iqbal et al. [11] and Saxena et al. [12] studies as mentioned in Table 2.

3.4. Numerical Modelling: Ballistic Impact with 7.62 AP Bullet

Ballistic impact with 7.62 AP bullet against base metal, weldment-1, and weldment-2 has been simulating by Abaqus 2017. The 2-dimensional model has been used for given purpose. Figure 3 shows the assembly of plate and bullet with dimensions. Plate dimensions are taken as 200 × 25 mm. In the case of bullet only steel core of bullet has been

modeled with 7.62 mm diameter. The upper and lower part of the plate has been fixed with the boundary condition I ($U_1 = U_2 = UR_3 = 0$) where U_1 and U_2 are the displacement in X and Y direction and UR_3 is the rotation in Z direction. Boundary condition II ($V_1 = 820$ m/s) has been applied on the bullet as a predefined velocity in X direction. Surface to surface interaction (with friction of coefficient = 0.23 and hard contact) has been given at the surface of bullet and plate where bullet surface is considered as master surface and plate surface is considered as slave surface. The boundary conditions with contact properties are shown in Figure 1. A four-node bilinear plane stress quadrilateral, reduced integration, hourglass control element CPS4R was used for meshing both bullet and plate as shown in Figure 4.

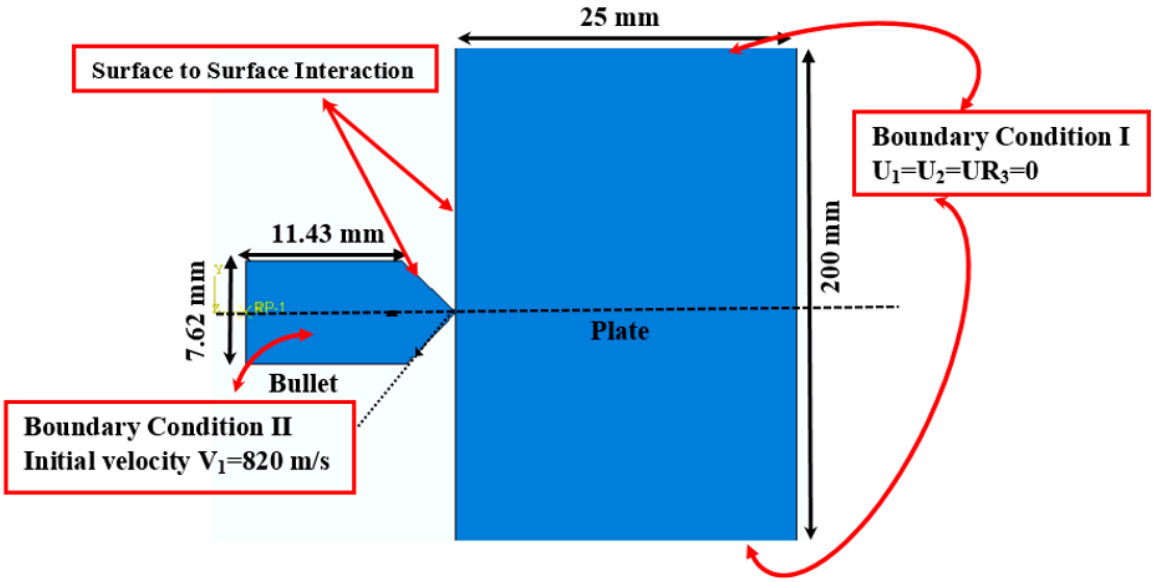

Figure 3. Assembly of Bullet and Plate.

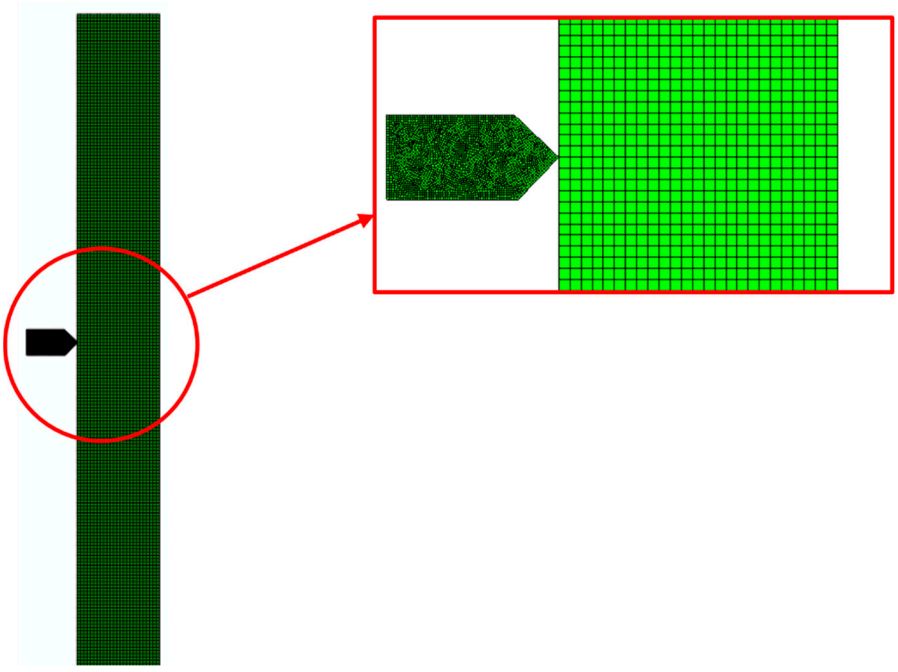

Figure 4. Meshing of 7.62 AP steel bullet core and target plate.

Bullet and plate both are make as deformable bodies. Bullet has been created an impact on the plate with a velocity of 820 m/s. At the same velocity Bullet strikes the base

metal, weldment-1 and weldment-2 plate. Bullet and plate have been contained the 2812 and 5220 elements respectively for analysis. Further, the number of nodes in bullet and plate are 2876 and 5446, respectively.

In the research of Rogers [17], Yildirim et al. [18], Ravichandran et al. [19], and Molinari et al. [20] revealed that more than 90% of the energy dissolved in the form of heat during expeditious plastic deformation in metals resulting in a temperature rise. Further, Rogers [17] revealed that the expeditious plastic deformation is adiabatic, and no heat loss takes place during the deformation. Several numerical simulations [17,21] proved that impacted surface temperature increases with an increase in impact velocities of the bullet. According to Yildirim et al. [18], Molinari et al. [20], Finney et al. [21], and Rosenberg et al. [22], bullets with a velocity range of 700–1000 m/s could rise the impacted surface temperature from 623 to 773 K. An approximate estimation of bullet impact against solid objects predicted that bullet energy increased the bullet temperatures beyond 1273 K after impact under ideal conditions.

A mesh convergence study also has been performed for the FEA model of base metal against 7.62 AP steel core. The mesh convergence study has been performed with 3249, 3743, 4265, 4768, and 5220 numbers of elements.

4. Result and Discussion

4.1. Depth of Penetration and Microstructural Investigation

Figure 5 shows the results of mesh convergence study of base metal plate FEA model. The results are plotted between depth of penetration vs. number of elements. Further, the results revealed that with the minimum number of elements, the size of element is increased, and after the deletion of elements, it shows a greater depth of penetration. The elements with 3249, 3743, and 4265 numbers show a greater depth of penetration. Further the depth of penetration becomes constant at 4768 and 5220 number of elements. The FEA results for all three investigating materials (base metal, weldment-1 and weldment-2) have been drawn with the highest number of elements, which is 5220.

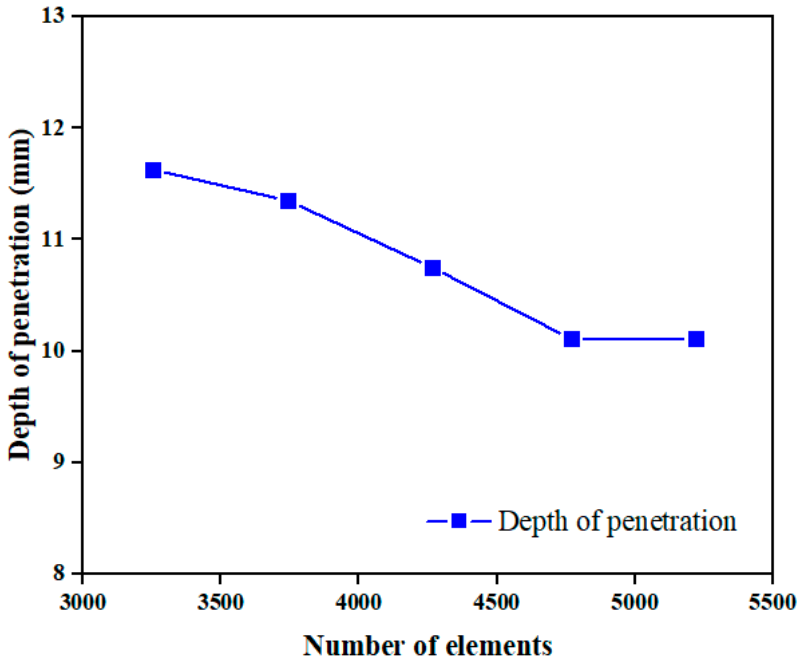

Figure 5. Depth of penetration vs. Number of elements.

The bullet elements with fewer than 2812 elements causes the access deformation at the nose section which results in the termination of explicit analysis. The FEA simulation results of the investigated materials have been drawn with the 2812 bullet elements.

Figure 6 shows the validation of FEA model depth of penetration results with the experimental results in the form of bar chart. The results are plots for the base metal, weldment-1 and weldment-2 against 7.62 AP bullet. Further, the experiments confirm the depth of penetration for base metal, weldment-1, and weldment-2 as 10.93, 13.65, and 15.20 mm, respectively, against 7.62 AP bullet. The developed FEA model predicts the depth of penetration for base metal, weldment-1 and weldment-2 is 10.11, 12.87, and 14.6. The percentage difference between experimental and FEA results for base metal, weldment-1 and weldment-2 is 8.11%, 5.71%, and 3.94% respectively. The percentage error less than 10% shows the good prediction capability of developed FEA model. Figure 7 shows the bullet penetration experiment cut section for the base metal, weldment-1, and weldment-2.

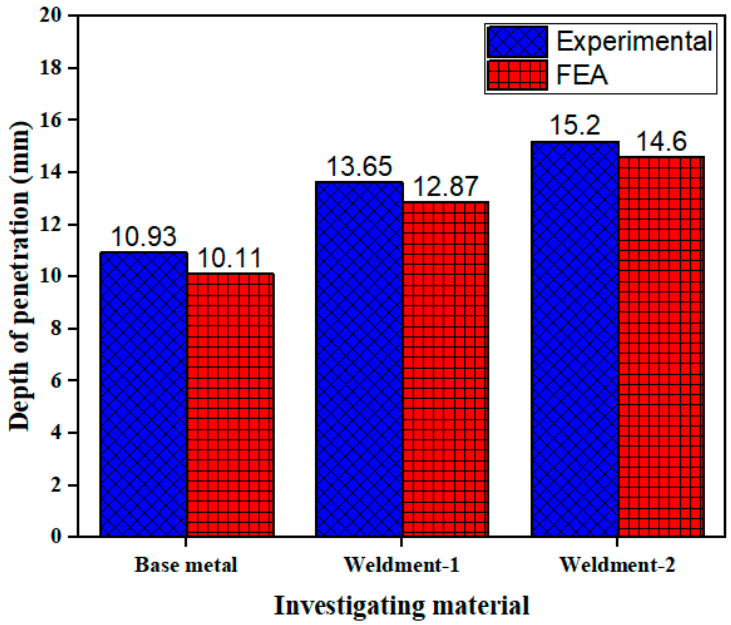

Figure 6. Experimental vs. FEA.

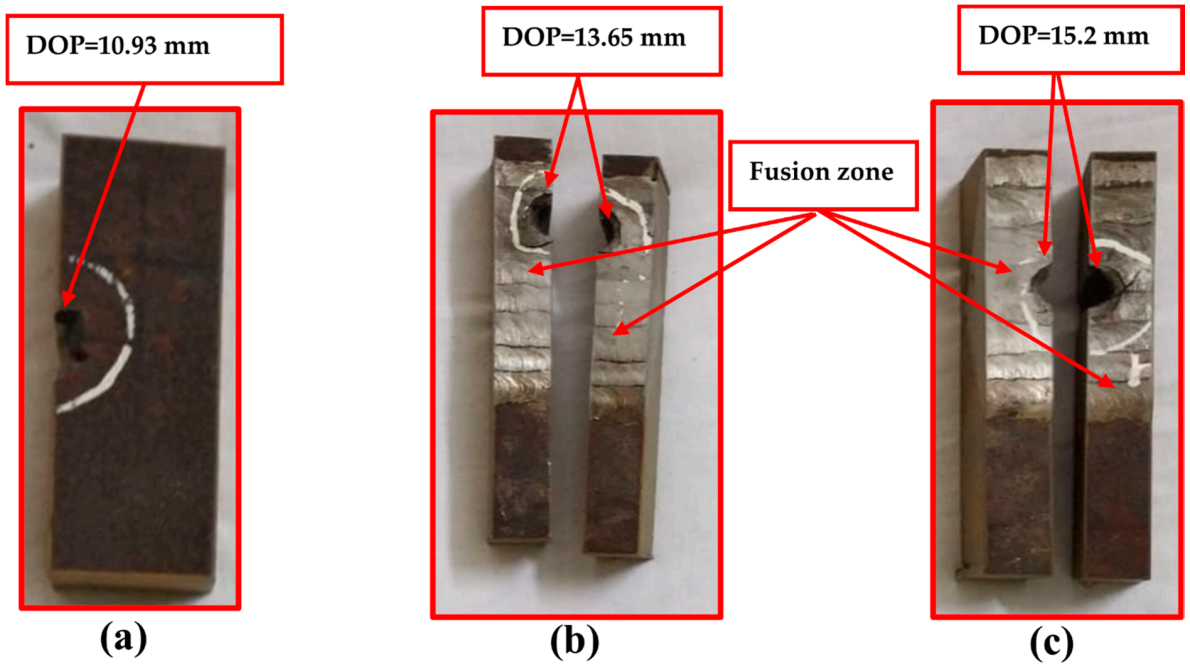

Figure 7. 7.62 AP bullet penetration cut section of (**a**) base metal, (**b**) weldment-1, (**c**) weldment-2.

Optical micrographs of fracture surface for base metal, weldment-1, and weldment-2 are shown in Figure 8a–c, respectively. In the present research, the thickness of the base metal plate and weldments is 25 mm and 7.62 AP bullet is not able to penetrate throughout. A clear denting is observed in the attack zone area in Figure 8a–c, which represents the inability of projectile in penetration of target plate. The more denting area is shown in Figure 8b (weldment-1) than Figure 8c (weldment-2).

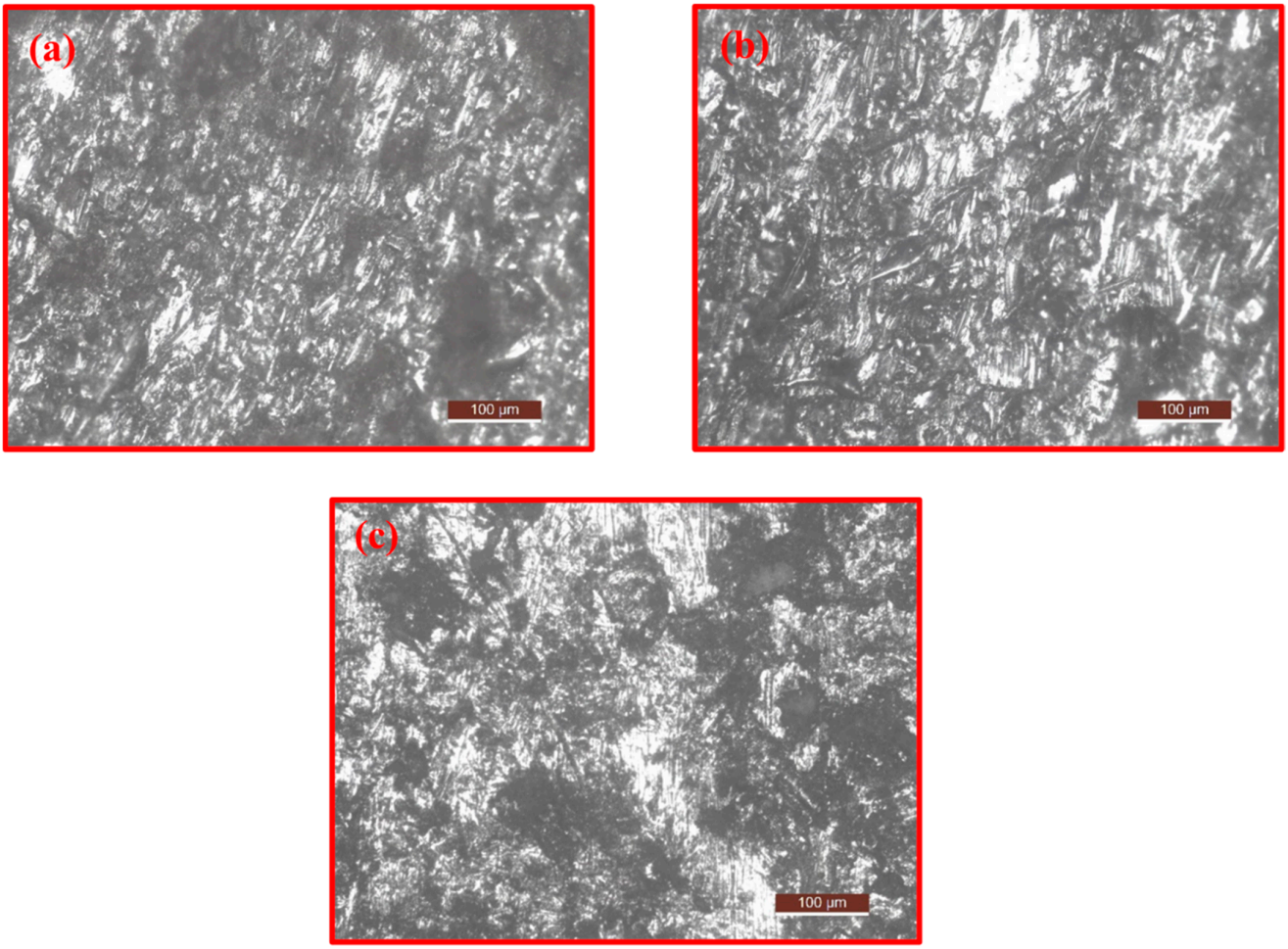

Figure 8. Fracture surface optical micrograph (**a**) base metal, (**b**) weldment-1, (**c**) weldment-2.

Further, the fragmentation failure has been identified in all three investigation materials. The all three investigation material micrographs exhibited the poor penetration ability. Further, the white-etched portion in Figure 8a–c represents the adiabatic shear bands.

Figure 9 Shows the finite element analysis (FEA) result of ballistic impact (7.62 AP bullet penetration) against base metal, weldment-1 and weldment-2 in terms of depth of penetration (DOP) at different step time. Three different selected time is 0, 25, and 500 µs. Further, the given time is the total step time for explicit simulation.

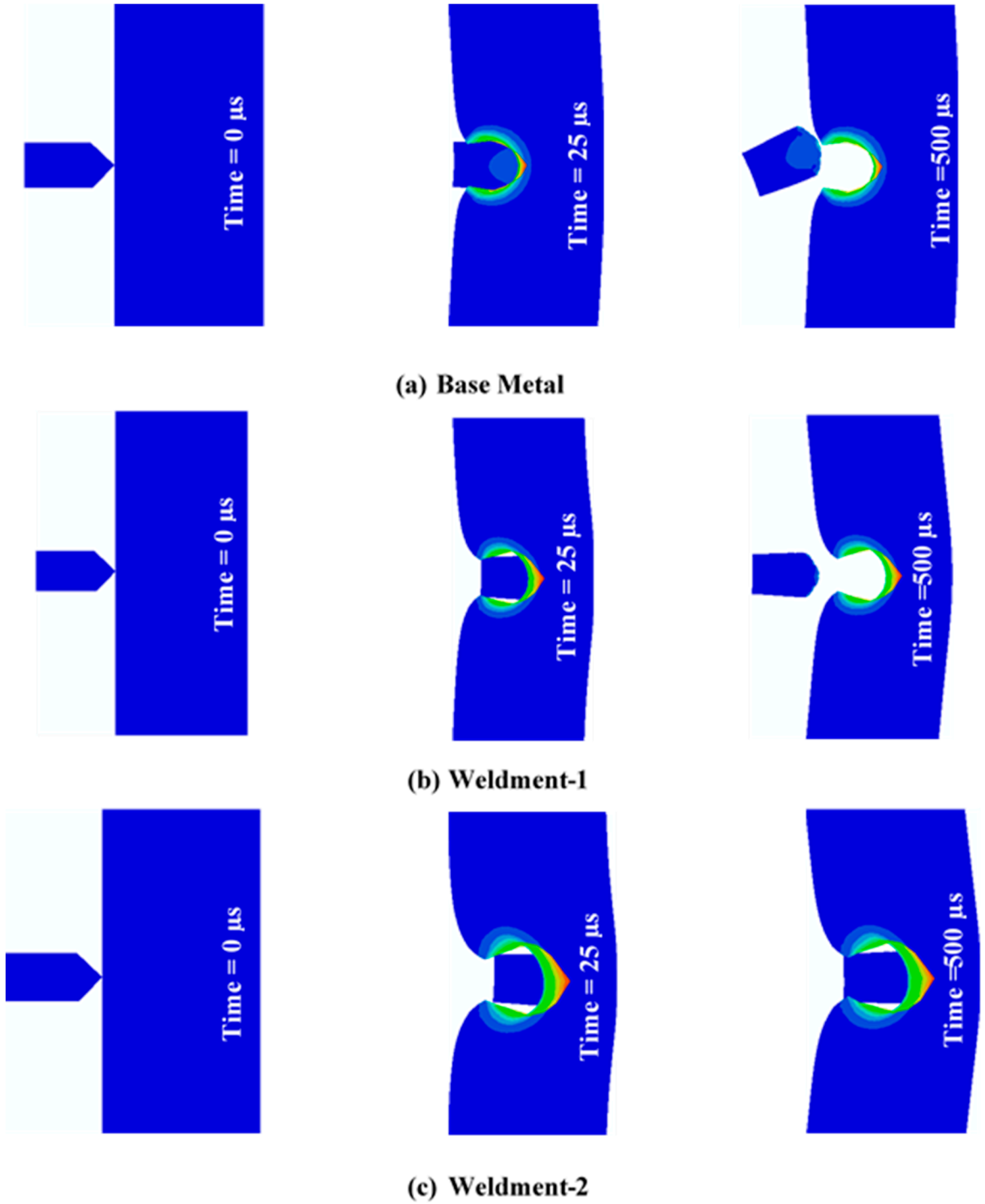

Figure 9. Depth of Penetration contours at different step time for (**a**) Base Metal, (**b**) Weldment-1, (**c**) Weldment-2.

Figure 9 Shows the visualization of FEA results. Figure 10 shows the graph between DOP vs. Time for all three under investigation materials. The ballistic resistance of base metal against 7.62 AP bullet is highest than remaining materials. Base metal, weldment-1 and weldment-2 has DOP of 10.11, 12.87, and 14.60 mm respectively. Weldment-1 has good ballistic resistance than weldment-2 which more DOP at same impact velocity of 820 m/s. The obtained results are in good agreement with the experimental studies of Saxena et al. [12] and Reddy et al. [23]. Saxena et al. [3] reveal that the weldment-1 consists of acicular ferrite in which each lath is divided by high boundary angle displaying fine grain size (typically 1–3 µm) usually possesses high strength compared to weldment-2.

The microstructure of fusion zone of weldment-2 consists of skeletal δ-ferrite in a plain austenitic matrix. The presence of high Ni (9.45%) in weldment-2 balances the austenitic structure against the formation of martensite.

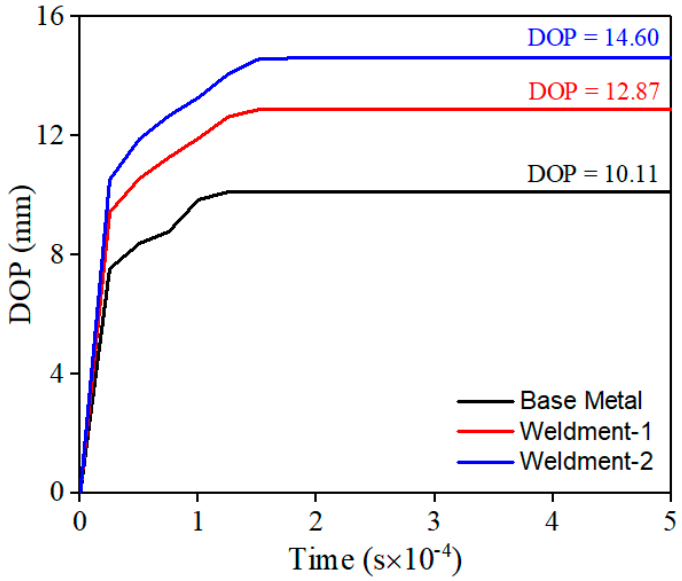

Figure 10. Depth of Penetration vs. Step time.

4.2. Impact Velocity vs. Time

Figure 11 shows the depth graph between impact velocity vs. time. In the present investigation, a comparative study of the resistance of penetration against 7.62 AP bullet between base metal, weldment-1, and weldment-2 is presented. For the given purpose a constant impact velocity of 820 m/s is considered for bullet. Generally, in practical applications the 7.62 AP bullet velocity is around 820 m/s. The trend of the graph is almost similar for all three materials under investigation. The bullet velocity is reduced with the increase of step time and almost equal to zero at the end of the step time. Complete penetration has not taken place in a single case in the present study.

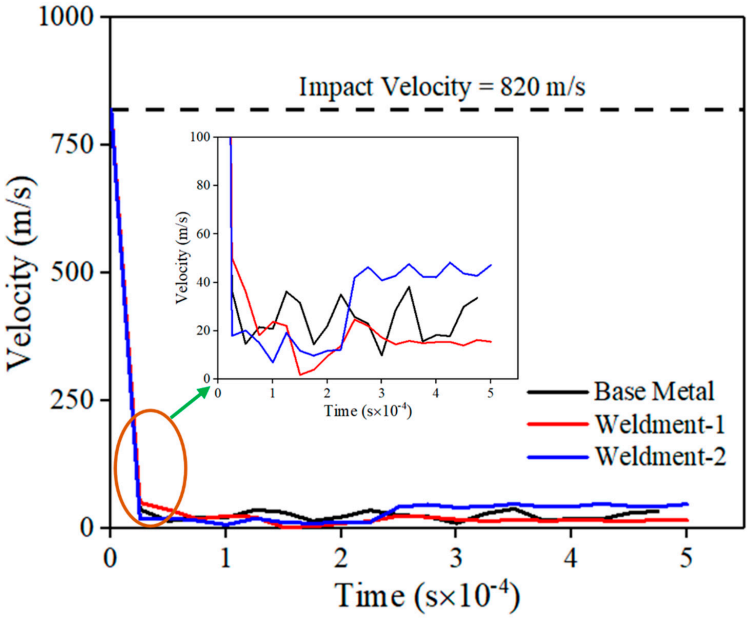

Figure 11. Velocity vs. Step time.

4.3. Feasibility of Weldment-1 over Weldment-2

Figures 9 and 10 show that weldment-1 has more resistance than weldment-2. One more point is that the cost of weldment-2 consumables is more in comparison to weldment-1. A recent investigation [3–7] proved that the tensile strength and yield strength of weldment-1 is more than weldment-2. However, the toughness of weldment-2 is comparatively higher in comparison of weldment-1 [3]. A similar type of trend is found in the fracture surface micrographs and weldment-1, which shows good performance against 7.62 AP bullet compared to weldment-2. The present study can thus state that weldment-1 prepared by LHF consumables can be used in place of weldment-2 prepared by ASS consumables in the SMAW of Armox 500T.

5. Conclusions

The FEA model of base metal, weldment-1, and weldment-2 shows a DOP of 10.11, 12.87, and 14.60 mm respectively against the 7.62 AP bullet, which shows the strong ballistic resistance of the base metal plate. Further, the experimental results show the DOP of base metal, weldment-1, and weldment-2 is 10.93, 13.65, and 15.20 mm, respectively, against 7.62 AP bullet. The FEA results ae in good agreement with experimental results within the percentage error of 10%, which shows the good prediction capability. A two-dimensional explicit model has been developed to reduce the processing and run time, which is greater in the three-dimensional model case. Weldment-1 shows greater strength to resist the penetration of a 7.62 AP bullet than weldment-2. Weldment-1 shows the more denting structure in fractured surface optical micrographs than weldment-2, which shows the greater toughness of weldment-1 compared to weldment-2. The present study thus made a recommendation that, in ballistic impact applications, the LHF consumables can be used in place of ASS consumables.

Author Contributions: Conceptualization, A.S., S.P.D., S.S.; Methodology, A.S., S.P.D., S.S.; Software, A.S.; Validation, A.S., S.S. and V.S.S.; Formal analysis, S.S. and V.S.S.; Investigation, G.S., J.S., and S.C.; Resources, S.S., and C.I.P.; Data curation, S.S., and C.I.P.; Writing—original draft preparation, A.S.; Writing—review and Editing, S.P.D.; Visualization, V.S.S.; Supervision, A.S., S.P.D., S.S., J.S., and S.C.; project administration, A.S., S.P.D., S.S., G.S., S.C., V.S.S. All authors have read and agreed to the published version of the manuscript.

Funding: This research received no external funding.

Institutional Review Board Statement: Not applicable.

Informed Consent Statement: This article does not contain any studies with human participants or animals performed by the author.

Data Availability Statement: No new data were created or analyzed in this study. Data sharing is not applicable to this article.

Conflicts of Interest: The authors declare no conflict of interest.

References

1. Zejian, X.; Huang, F. Plastic behavior and constitutive modeling of armor steel over wide temperature and strain rate ranges. *Acta. Mech. Solida Sin.* **2012**, *25*, 598–608.
2. Barényi, I.; Híreš, O.; Lipták, P. Changes in mechanical properties of armoured UHSLA steel ARMOX 500T after over tempering. *Probl. Mech. Armament Aviat. Saf. Eng.* **2013**, *4*, 7–14.
3. Saxena, A.; Kumaraswamy, A.; Reddy, G.M.; Madhu, V. Influence of welding consumables on tensile and impact properties of multi-pass SMAW Armox 500T steel joints vis-a-vis base metal. *Def. Technol.* **2018**, *14*, 188–195. [CrossRef]
4. Saxena, A.; Kumaraswamy, A.; Sethi, S.; Reddy, G.M.; Madhu, V. Microstructural Characterization and High Strain Rate Plastic Flow Behavior of SMAWArmox500T Steel Joints from Spherical Indentation Experiments. *J. Mater. Eng. Perform* **2018**, *27*, 4261–4269. [CrossRef]
5. Saxena, A.; Kumaraswamy, A.; Vemuri, M. Investigation of S-D effect on plastic flow behavior of Armox 500T steel. *J. Braz. Soc. Mech. Sci. Eng.* **2018**, *40*, 463. [CrossRef]
6. Saxena, A.; Kumaraswamy, A. Numerical Analysis of Effect of Temperature on Ball Indentation Behavior of Armox500T and IN718. *Trans. Indian Inst. Met.* **2018**, *71*, 3111–3116. [CrossRef]

7. Zukas, J.A. *High Velocity Impact Dynamics*; Wiley: New York, NY, USA, 1990.
8. Reddy, G.M.; Mohandas, T. Ballistic performance of high-strengh low-alloy steel weldments. *J. Mater. Process. Technol.* **1996**, *57*, 23–30. [CrossRef]
9. Reddy, G.M.; Mohandas, T.; Papukutty, K. Effect of welding process on the ballistic performance of high-strength low-alloy steel weldments. *J. Mater. Process. Technol.* **1998**, *74*, 27–35. [CrossRef]
10. Pramanick, A.; Das, H.; Reddy, G.; Ghosh, M.; Das, G.; Nandy, S.; Pal, T. Development and design of microstructure based coated electrode for ballistic performance of shielded metal arc welded armour steel joints. *Mater. Des.* **2016**, *103*, 52–62. [CrossRef]
11. Iqbal, M.; Senthil, K.; Sharma, P.; Gupta, N. An investigation of the constitutive behavior of Armox 500T steel and armor piercing incendiary projectile material. *Int. J. Impact Eng.* **2016**, *96*, 146–164. [CrossRef]
12. Saxena, A. Comparative Study of Effect of Strain-Rate on Plastic Flow Behavior of Armor Steel Weldments for Defence Applications. Ph.D. Thesis, Defence Institute of Advanced Technology, Pune, India, May 2019.
13. Børvik, T.; Dey, S.; Clausen, A. Perforation resistance of five different high-strength steel plates subjected to small-arms projectiles. *Int. J. Impact Eng.* **2009**, *36*, 948–964. [CrossRef]
14. Johnson, G.R.; Cook, W.H. A constitutive model and data for metals subjected to large strains, high strain rates and high temperatures. In Proceedings of the 7th International Symposium on Ballistics, Hague, The Netherlands, 19–21 April 1983; Volume 21, pp. 541–547.
15. Johnson, G.R.; Cook, W.H. Fracture characteristics of three metals subjected to various strains, strain rates, temperatures and pressures. *Eng. Fract. Mech.* **1985**, *21*, 31–48. [CrossRef]
16. Hancock, J.; MacKenzie, A. On the mechanisms of ductile failure in high-strength steels subjected to multi-axial stress-states. *J. Mech. Phys. Solids* **1976**, *24*, 147–160. [CrossRef]
17. Rogers, H.C. Adiabatic Plastic Deformation. *Annu. Rev. Mater. Res.* **1979**, *9*, 283–311. [CrossRef]
18. Yildirim, B.; Muftu, S.; Gouldstone, A. Modeling of high velocity impact of spherical particles. *Wear* **2011**, *270*, 703–713. [CrossRef]
19. Ravichandran, G.; Rosakis, A.J.; Hodowany, J.; Rosakis, P. On the Conversion of Plastic Work into Heat During High-Strain-Rate Deformation. *Fourth Huntsville Gamma Ray Burst Symp.* **2002**, *620*, 557–562. [CrossRef]
20. Molinari, J.; Ortiz, M. A study of solid-particle erosion of metallic targets. *Int. J. Impact Eng.* **2002**, *27*, 347–358. [CrossRef]
21. Finney, M.A.; McAllister, S.S.; Maynard, T.B.; Grob, I.J. A Study of Wildfire Ignition by Rifle Bullets. *Fire Technol.* **2015**, *52*, 931–954. [CrossRef]
22. Rosenberg, Z.; Dekel, E. *Terminal Ballistics*; Springer: Berlin, Germany, 2012; pp. 267–291.
23. Reddy, G.M.; Mohandas, T.; Tagore, G. Weldability studies of high-strength low-alloy steel using austenitic fillers. *J. Mater. Process. Technol.* **1995**, *49*, 213–228. [CrossRef]